Quantum Tunneling Mediated Interfacial Synthesis of a Benzofuran Derivative

Tobias Paintner[+], Jonas Björk[+],* Ping Du, Svetlana Klyatskaya, Mateusz Paszkiewicz, Raphael Hellwig, Martin Uphoff, Murat A. Öner, Edoardo Cuniberto, Peter S. Deimel, Yi-Qi Zhang, Carlos-Andres Palma, Francesco Allegretti, Mario Ruben, Johannes V. Barth, and Florian Klappenberger*

Abstract: *Reaction pathways involving quantum tunneling of protons are fundamental to chemistry and biology. They are responsible for essential aspects of interstellar synthesis, the degradation and isomerization of compounds, enzymatic activity, and protein dynamics. On-surface conditions have been demonstrated to open alternative routes for organic synthesis, often with intricate transformations not accessible in solution. Here, we investigate a hydroalkoxylation reaction of a molecular species adsorbed on a Ag(111) surface by scanning tunneling microscopy complemented by X-ray electron spectroscopy and density functional theory. The closure of the furan ring proceeds at low temperature (down to 150 K) and without detectable side reactions. We unravel a proton-tunneling-mediated pathway theoretically and confirm experimentally its dominant contribution through the kinetic isotope effect with the deuterated derivative.*

The tunneling of massive particles through potential barriers exceeding the particle energy is a fundamental concept of quantum mechanics and has significant impact on important processes in nature. It is essential for explaining the spectroscopic term schemes of molecules, for example, in the case of ammonia reported by Hund in 1927.[1] In 1933 Bell already realized that tunneling can significantly contribute to the kinetic isotope effect (KIE) in hydrogen transfer reactions, rendering a quantum-mechanical treatment essential for their description.[2] More recently, it was demonstrated that quantum tunneling can be responsible for the fast decay of compounds,[3] direct reactions to products not accessible through classical pathways,[4] and enable chemical conversions in extreme (e.g. interstellar) environments.[5] Furthermore, the implications of tunneling-mediated reactions extend into biology, where quantum mechanical hydrogen transfer can cause mutations that possibly lead to cancer and other diseases[6] and influence enzyme activity.[7] On atomically well-defined surfaces, proton tunneling has been hitherto reported to impact elementary processes such as diffusion,[8] structural dynamics,[9] tautomerization,[10] desorption,[11] and hydrogenation.[12] However, in contrast to the plethora of complex, covalent reactions reported in the context of surface-assisted synthesis and heterogeneous catalysis, tunneling-mediated reaction pathways have remained elusive.

Over the past few decades, intramolecular cyclization leading to the synthesis of biologically relevant heterocyclic compounds[13] has gained much attention as one of the simplest and most efficient methods for constructing furan ring systems.[14] Alkynylbenzene derivatives with a nucleophilic site at the *ortho* position, such as *o*-alkynylphenols or *o*-alkynylphenyl ethers, are widely utilized as efficient precursors for constructing benzofurans. A number of methods using bases as well as transition or noble metal catalysts have been established for C−O cyclization.[15]

Here, we investigate the chemical conversion of a 4″-diethynyl-5,5″-dihydroxy-(1,1′:4′,1″-terphenyl)-3,3″-dicarbonitrile compound (Figure 1a, **1**) on a noble metal surface by means of multi-technique characterization. We find a highly selective hydroalkoxylation reaction, which intriguingly proceeds well below room temperature. A modeling analysis, based on density functional theory (DFT), identifies the underlying proton-tunneling-mediated pathway. In agreement, the KIE assessment confirms the quenching of the tunneling-mediated reaction for a deuterated isomer. Our work provides clear evidence for the tunneling-mediated

[*] Dr. T. Paintner,[+] M. Paszkiewicz, Dr. R. Hellwig, M. Uphoff,
M. A. Öner, E. Cuniberto, Dr. P. S. Deimel, Dr. Y.-Q. Zhang,
Prof. Dr. C.-A. Palma, Dr. F. Allegretti, Prof. Dr. J. V. Barth,
Dr. F. Klappenberger
Physics Department E20, Technical University of Munich
85748 Garching (Germany)
E-mail: florian.klappenberger@tum.de

Dr. J. Björk[+]
Department of Physics, Chemistry and Biology, IFM
Linköping University
58183 Linköping (Sweden)
E-mail: jonas.bjork@liu.se

Dr. P. Du, Dr. S. Klyatskaya, Prof. Dr. M. Ruben
Institute of Nanotechnology
Karlsruhe Institute of Technology (KIT)
Hermann-von-Helmholtz-Platz 1
76344 Eggenstein-Leopoldshafen (Germany)

Prof. Dr. C.-A. Palma
Institute of Physics, Chinese Academy of Sciences
100190 Beijing (P. R. China)

Prof. Dr. M. Ruben
Institute de Physique et Chimie de Matériaux (IPCMS)
Université Strasbourg
23 rue du Loess, BP 43, 67034 Strasbourg cedex 2 (France)

[+] These authors contributed equally to this work.

🖳 Supporting information and the ORCID identification numbers for
ⓘD some of the authors of this article can be found under:
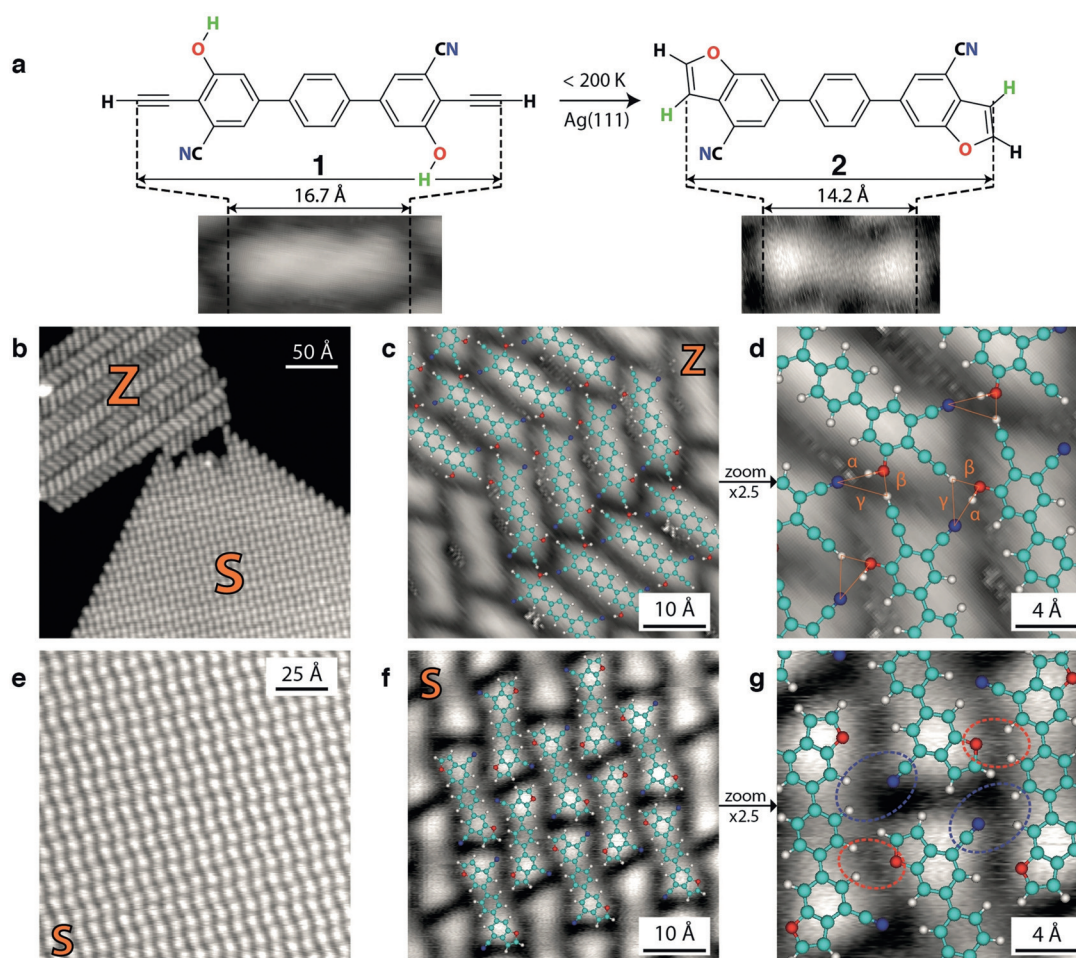https://doi.org/10.1002/anie.201904030.

Figure 1. Conversion of a molecular assembly through on-surface hydroalkoxylation. a) Lewis structures of **1** and **2** showing the hydroalkoxylation reaction and typical STM appearance of the respective species. b–g) STM topographs after b–d) deposition at $T_{sub} = 100$ K followed by annealing at $T_{ann} = 250$ K ($V_B = -1.0$ V, $I_T = 0.1$ nA), and e–g) further annealing at $T_{ann} = 400$ K ($V_B = -1.0$ V, $I_T = 30$ pA). c,d,f,g) Close-up STM images with superposed molecular models. c) Intermolecular bonding scheme proposed for Z domains. d) Close-up image of a Z domain. ($V_B = 300$ mV, $I_T = 100$ pA). f) Intermolecular bonding scheme proposed for S domains. g) Close-up of an S domain. ($V_B = 10$ mV, $I_T = 50$ pA, $T_{ann} = 400$ K).

pathway dominantly influencing the complex on-surface reaction.

We achieved the de novo synthesis of compound **1** (see Figure S1 in the Supporting Information) with three different functional groups (−C≡N, −OH, and −C≡CH). The molecule was deposited onto a Ag(111) surface held at $T_{sub} \approx 100$ K. Irregular aggregates of the precursor were subsequently observed in the scanning tunneling microscopy (STM) images (Figure S2) obtained at $T_{meas} \approx 4.5$ K (the same temperature was used to record all the images presented). The data indicate that limited diffusion prevents the formation of regular molecular assemblies, so that species **1** remains pristine. Annealing the sample to an intermediate temperature ($T_{ann} = 250$ K) led to the formation of two distinct regular assemblies that coexist in segregated islands (Figure 1 b). These arrangements are referred to as the zigzag (Z) and snake (S) phases, respectively. The two phases exhibit markedly different intramolecular contrast in the STM images (highlighted in the lower panels of Figure 1 a). Furthermore, they are clearly distinguishable by their unit cell parameters and their orientations with respect to the

high-symmetry directions of the substrate (Figure S3). After further thermal treatment at $T_{ann} = 400$ K, the S-phase remains exclusively (Figure 1 e). The evolution from phase Z into phase S is associated with a gradual chemical conversion from species **1** into **2,** as depicted in Figure 1 a. Recent reports on covalent transformations of precursors with similar functional groups[16] suggest that the alkyne and hydroxy moieties undergo a hydroalkoxylation reaction, whereby the functional groups fuse into a five-membered ring together with the involved part of the nearby phenyl ring, thus creating a furan moiety.

Modeling the STM data with scaled molecular units supports our hypothesis that the original precursor **1** (Figures 1 c,d) is converted into product **2** (Figures 1 f,g). The arrangement within Z domains can be rationalized by hydrogen bonding through O−H···N, C−H···O, and C−H···N interactions (denoted as α, β, γ in Figure 1 d). The S assemblies optimize interactions between the potential proton acceptors O and N and nearby organic rings (red and blue outlines in Figure 1 g).[17] Notably, attempts to explain the S phase with intact reactants **1** result in clearly prohibitive steric constraints

(see Figure S3c,d). Force-field simulations of extended aggregates of species **1** and **2** on a substrate (Figure S4) corroborate the arrangement modes of both assemblies derived from the structural analysis.

To elucidate the chemical structure of the newly formed species as well as the reaction involved, we employed complementary spectroscopic techniques to assess the chemical shifts of the atomic constituents and the molecular orbital properties before and after the reaction. First, we performed X-ray photoelectron spectroscopy (XPS, see also the Supporting Information) and analyzed the O 1s region of a series of samples exposed to the same amount of **1** and annealed to increasing temperatures (Figure 2a). For $T_{ann} = 200$ K, we observed a broad O 1s peak containing two convoluted components. The binding energies E_B of these two peaks are 533.6 and 534.3 eV, which agree well with literature values for phenol and furan species adsorbed on Ag surfaces.[18] Annealing freshly prepared samples at higher temperatures results in an increased intensity of the furan contribution, which becomes prevalent at $T_{ann} = 350$ K. The XPS data thus not only support the proposed hydroalkoxylation scenario, but also exclude deprotonation of the hydroxy group as a dominant effect,[19] since prominent features between 532 and 530 eV are absent.

Whereas all the atoms of the reactant are still present in the products in the case of hydroalkoxylation, alternative

Figure 2. Element-specific identification of the furan ring-closure by X-ray electron spectroscopy. a) Comparison of the O 1s XPS signature for different annealing temperatures, which trigger the conversion of **1** into **2**. b) NEXAFS C K-edge spectra, taken at an incidence angle (definition see inset) of $\theta = 90°$, for a non-annealed (black) and an annealed (red) sample with sub-monolayer coverage. Experimental data (lower curves) are compared to simulated spectra (upper curves).

conversions involving substrate-mediated cracking would result in desorption of the abstracted subunits. Thus, temperature-programmed desorption (TPD) was employed to test for potential molecular fragmentation. In multiple heating ramps carried out after the adsorption of various coverages of species **1** at 100 K, we detected neither small fragments (atomic mass < 50) nor any molecular or atomic H (Figure S5) that could be associated with dehydrogenation processes. Accordingly, the TPD investigation implies proton abstraction cannot explain the chemical conversion and supports the hydroalkoxylation scenario.

Near-edge X-ray absorption fine-structure (NEXAFS) data were collected for further characterization of the reactants and products. We compared the angle-dependent C K-edge spectra of a sample prepared by deposition of **1** at $T_{sub} = 120$ K with the spectra of the same sample after annealing to 400 K (Figure 2b and Figure S6a,b). We chose an incident angle $\theta = 90°$, as it is sensitive to the in-plane π systems of the CN and the CCH moieties. To distinguish contributions from different molecular orbitals, we performed DFT C K-edge spectra simulation for species **1** and **2** (Figure 2b; see also Figure S6c,d). For the deposition at 120 K, the resonance at 285 eV originates from the phenyl moieties in the molecular backbone (see Figure S6a,b) and the pronounced dichroism reveals an overall near-to-flat adsorption geometry. The simulated NEXAFS spectrum of **1** (black curves in Figure 2b, see also Figure S6a,c) reproduces the double structure of feature A and the sharper peak B originating from the CCH and CN moieties, respectively. Thus, the data confirm the integrity of the precursor under such conditions. The dichroism at 285 eV is preserved (Figure S6b) after annealing at 400 K, which indicates that the flat adsorption geometry is maintained for the new species, in agreement with the modeling of the STM data. Furthermore, the feature B is retained in the spectrum (lower red curve in Figure 2b), which indicates that the CN group is not perturbed upon annealing, as its in-plane π* orbital is preserved. In contrast, the spectral signature around 286 eV (CCH, labeled A), which corresponds to the in-plane π* resonance of the terminal alkyne group is quenched, indicative of the conversion of the C≡C bond to a double bond. These three key features also nicely match the simulated spectra of the proposed species **2** (upper red curve in Figure 2b, see also Figure S6d). Therefore, the good agreement between simulated and experimental NEXAFS data in conjunction with the other observations provides conclusive evidence for the proposed hydroalkoxylation scenario.

To analyze and rationalize the reaction mechanism, we carried out DFT-based harmonic transition state theory (HTST) calculations, using a simplified molecule with the central phenyl ring of **1** omitted. The most favorable free energy pathway calculated for $T = 200$ K is depicted in Figure 3a (blue line). The two-step reaction proceeds through a hydrogen transfer from the hydroxy to the alkyne group (**IS** to **IntS**), which proceeds through the transition state **TS1**, followed by a ring-closing reaction by rotation of the involved C_2H_2 moiety (**IntS** to **FS**) to form the furan moiety. Importantly, the intermediate state **IntS**, where the original ethynyl group is effectively converted into an ethenylene,
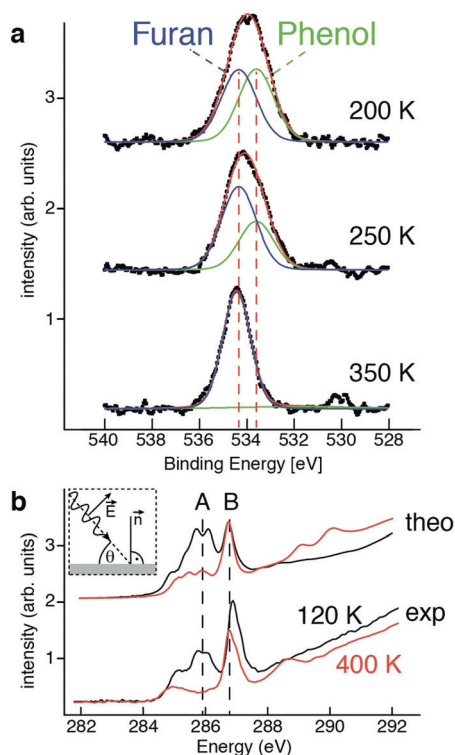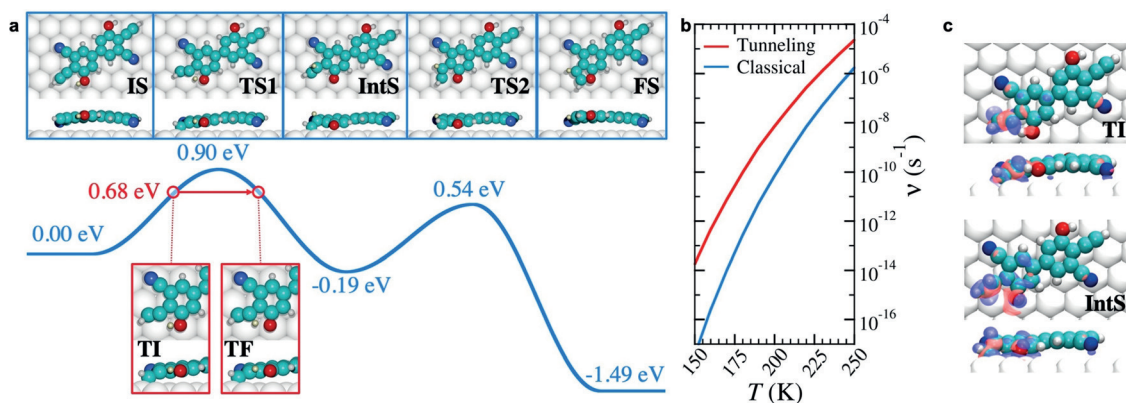
Figure 3. Computational modeling of the cyclization mechanism. a) Scheme of the reaction pathway obtained from DFT-based HTST calculations, with the free energy profile of the classical (lowest energy) pathway shown in blue and the tunneling pathway in red. Top and side views of local minima referred to as initial, intermediate, and final state (**IS**, **IntS**, **FS**). Transition states (**TS1**, **TS2**) are also shown as well as a zoom-in of the quantum tunneling turning points (**TI**, **TF**). b) Comparison of the reaction rates of the classical and tunneling-mediated pathways going from **IS** to **IntS**, with the axis for the rates scaled logarithmically. c) Plots of the electron density difference for **TI** and **IntS**, showing electron redistribution as a result of the molecule–surface interactions, where blue (red) indicates electron accumulation (depletion). The absolute value of the contours is 0.01 e Å^{-3}.

becomes favorable through the presence of the substrate, which enables bonding of the outermost carbon atom to surface atoms (see side view of **TS1**). In the HTST scenario, the classical reaction rate for $T = 200$ K with a free energy of activation $\Delta G^{\ddagger}$ of 0.903 eV can be calculated by the Eyring equation as $\nu_C = \frac{k_B T}{h} \exp\left(-\frac{\Delta G^{\ddagger}}{k_B T}\right) \approx 7 \times 10^{-11}$ s^{-1}.

This minute value implies that in a classical picture, the reaction should not proceed. Considering that its initial step is crucially influenced by a proton transfer, we investigated the role of quantum tunneling in this process. Examining the vicinity of **TS1** with the de novo approach detailed in the Supporting Information (see Section M6), we indeed isolated two states suitable for proton tunneling, namely, having the same energy and differing in structure only by the position of the H atom involved in the first reaction step. For transitioning between these states, the H atom has to move by only 0.60 Å, which suggests that the states can serve as so-called turning points, that is, positions where the mode of motion turns from classical behavior to quantum tunneling. The probability P of the related tunneling-mediated proton transfer process between the initial (**TI**) and final (**TF**) state (see Figure 3a, red states) was calculated with the WKB approximation across the barrier obtained by a linear translation of the H atom from **TI** to **TF**, and integrating between the energy of the initial tunneling point $\Delta G_{TI} = 0.68$ eV (for $T = 200$ K) and the maximum energy of the tunneling channel $\Delta G_T^{\ddagger} = 0.97$ eV. This is higher than the energy of the classical pathway **TS1** due to the constraints of the tunneling channel. We assumed that the tunneling barrier height is temperature-independent. The rate of the thermally assisted tunneling process was calculated by integrating over the free energies between ΔG_{TI} and $\Delta G_T^{\ddagger}$ according to Equation (1).

$$\nu_T = \frac{k_B T}{h} \int_{\Delta G_{TI}}^{\Delta G_T^{\ddagger}} \exp\left(-\frac{\Delta G}{k_B T}\right) \frac{P(\Delta G)}{k_B T} d\Delta G. \qquad (1)$$

In Figure 3b, it is clear that the tunneling-mediated rate ν_T exceeds the classical rate ν_C significantly throughout the relevant temperature range. Consequently, this relation implies a crucial role of proton tunneling in the reaction pathway. For example, at $T = 200$ K the quantum tunneling corrected rate is increased by a factor of about 100. Although the resulting reaction rate ν_T is still relatively small (7×10^{-9} s^{-1} at 200 K), it just represents a lower limit for several reasons: As the rate depends exponentially on the energy at the turning point ΔG_{TI}, more appropriate turning points could enhance the rate of the tunneling pathway further. Furthermore, we are considering just one tunneling channel, instead of integrating over the entire phase space of the reaction, which is well beyond our computational reach. However, the decisive insight is the existence of a tunneling channel, which opens a route for the proton transfer that is significantly more efficient than the classical pathway.

Importantly, the calculations also unveil the crucial role of the Ag(111) surface: At the turning points (**TI**, **TF**) the terminating C atom of the original ethynyl group interacts chemically with the surface, stabilizing both these states as well as the identified intermediate state **IntS**, thus allowing two turning points to come close enough in configurational space and be at the same time sufficiently low in energy. The chemical role of the surface is exemplified for **TI** and **IntS** in Figure 3c, by the differences in the electron density ($\Delta\rho = \rho_{mol@Ag(111)} - \rho_{Ag(111)} - \rho_{mol}$) caused by molecule–surface interactions. For **TI**, there is a strong accumulation of electrons between the terminating C atom and a surface atom. **TF** has similar characteristics (see Figure S11). Furthermore, for **TI** there is an accumulation of electrons between the tunneling proton and the terminal alkyne, which indicates that the surface-induced charge redistribution promotes the tunneling process. For **IntS**, there is an accumulation of electrons around the carbonyl oxygen atom, thus indicating its chemical interaction with the substrate.

In view of the modeling insights, we experimentally cross-checked the proton-tunneling-mediated reaction by examining the KIE with a deuterated isomer (i.e. deuterated hydroxy groups, see **1D** in Figure 4). Figures 4a and b depict STM topographs of comparable coverages of **1** and **1D** on Ag(111) annealed to 225 K (cf. also Figures S7 and S8). The Z and S phases clearly coexist for **1**, whereas for **1D** we find exclusively the Z assembly. The absence of the S phase is ascribed to a massively reduced probability of deuterium tunneling, whence the ring-closure process is inhibited. For a quantification of the KIE, we analyzed a large set of STM images and found 50 % reacted molecules for **1**, in contrast to only spurious features for **1D** well below 5 %. All other molecules were found to be intact, that is, assembled in the Z phase. This result sets a conservative lower limit for the KIE, namely the ratio of reaction rates of **1** and **2**, of 10 at 225 K, clearly indicating proton tunneling in the hydroalkoxylation reaction of **1**.[20] Further examination of the KIE was obtained from XPS data. An example is depicted in Figure 4c, where the furan-related component that dominates after annealing **1** at 250 K is practically absent in the **1D** sample. The minor component at lower E_B is attributed to impurities resulting from the preparation of the hygroscopic powder; see the Supporting Information. Consistently, an evaluation of the temperature dependence of the KIE from the combined STM and XPS data (Figure S9a) indicates its prominent role in the sub-300 K regime. During the investigation of the reaction rates we also noticed a high sensitivity to preparation conditions, which are consistent with the tunneling process (for details see Section A3 in the Supporting Information).

In conclusion, through investigating a hydroalkoxylation reaction under on-surface conditions we have demonstrated that proton-tunneling-mediated mechanisms enable highly selective complex reactions via pathways inaccessible through conventional approaches. Our findings shine light on tunneling reactions, especially under interfacial conditions. With proper pre-positioning and precursor design, it should be feasible to develop procedures to steer intermolecular tunneling-mediated coupling under extreme conditions and help to engineer the construction of atomically precise nanomaterials by a bottom-up approach. In general, the extraordinary sensitivity to the local environment surrounding the reactive site paves the way toward novel approaches to chemical reactions and quantum processes.
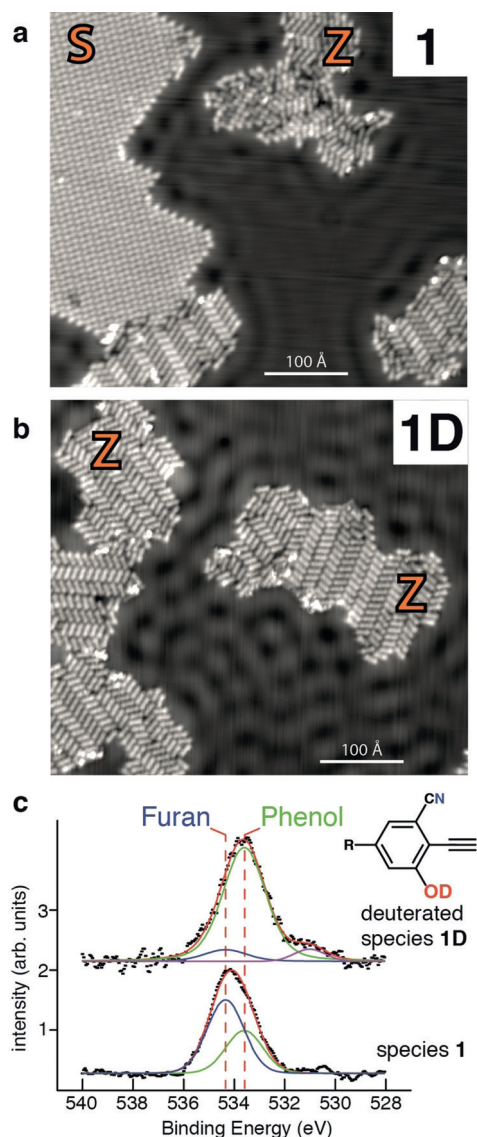

Figure 4. Isotope dependence of the benzofuran formation. Comparison of STM data ($V_B = -1.0$ V, $I_T = 0.1$ nA) after annealing at 225 K for a) the non-deuterated reactant **1** and b) its deuterated derivative **1D**. c) Comparison of the XPS O1s data of **1** and **1D** after annealing at 250 K. The binding energies of the furan- and phenol-related moieties are marked by vertical lines.

Conflict of interest

The authors declare no conflict of interest.

[1] F. Hund, *Z. Phys.* **1927**, *43*, 805–826.

[2] R. P. Bell, *Proc. R. Soc. London Ser. A* **1933**, *139*, 466–474.

[3] P. R. Schreiner, H. P. Reisenauer, F. C. Pickard Iv, A. C. Simmonett, W. D. Allen, E. Mátyus, A. G. Császár, *Nature* **2008**, *453*, 906–909.

[4] P. R. Schreiner, H. P. Reisenauer, D. Ley, D. Gerbig, C.-H. Wu, W. D. Allen, *Science* **2011**, *332*, 1300–1303.

[5] a) T. P. Goumans, J. Kästner, *Angew. Chem. Int. Ed.* **2010**, *49*, 7350–7352; *Angew. Chem.* **2010**, *122*, 7508–7511; b) R. J. Shannon, M. A. Blitz, A. Goddard, D. E. Heard, *Nat. Chem.* **2013**, *5*, 745–749; c) T. Hama, N. Watanabe, *Chem. Rev.* **2013**, *113*, 8783–8839.

[6] P.-O. Löwdin, *Rev. Mod. Phys.* **1963**, *35*, 724–732.

[7] a) Y. Cha, C. J. Murray, J. P. Klinman, *Science* **1989**, *243*, 1325–1330; b) L. Masgrau, A. Roujeinikova, L. O. Johannissen, P. Hothi, J. Basran, K. E. Ranaghan, A. J. Mulholland, M. J. Sutcliffe, N. S. Scrutton, D. Leys, *Science* **2006**, *312*, 237–241.

[8] L. Lauhon, W. Ho, *Phys. Rev. Lett.* **2000**, *85*, 4566–4568.

[9] a) A. D. Jewell, G. Peng, M. F. Mattera, E. A. Lewis, C. J. Murphy, G. Kyriakou, M. Mavrikakis, E. C. H. Sykes, *ACS Nano* **2012**, *6*, 10115–10121; b) X. Meng, J. Guo, J. Peng, J. Chen, Z. Wang, J.-R. Shi, X.-Z. Li, E.-G. Wang, Y. Jiang, *Nat. Phys.* **2015**, *11*, 235–239.

[10] M. Koch, M. Pagan, M. Persson, S. Gawinkowski, J. Waluk, T. Kumagai, *J. Am. Chem. Soc.* **2017**, *139*, 12681–12687.

[11] T. Minato, S. Kajita, C.-L. Pang, N. Asao, Y. Yamamoto, T. Nakayama, M. Kawai, Y. Kim, *ACS Nano* **2015**, *9*, 6837–6842.

[12] a) A. Hellman, E. J. Baerends, M. Biczysko, T. Bligaard, C. H. Christensen, D. C. Clary, S. Dahl, R. van Harrevelt, K. Honkala, H. Jonsson, G. J. Kroes, M. Luppi, U. Manthe, J. K. Norskov, R. A. Olsen, J. Rossmeisl, E. Skulason, C. S. Tautermann, A. J. C. Varandas, J. K. Vincent, *J. Phys. Chem. B* **2006**, *110*, 17719–17735; b) C. S. Tautermann, D. C. Clary, *J. Chem. Phys.* **2005**, *122*, 134702.

[13] H. Khanam, Shamsuzzaman, *Eur. J. Med. Chem.* **2015**, *97*, 483–504.

[14] a) E. J. Thomas in *Science of Synthesis*, *Vol. 10* (Ed.: E. J. Thomas), Georg Thieme Verlag, Stuttgart, **2000**, pp. 916–927; b) L. Chen, K. Chen, S. Zhu, *Chem* **2018**, *4*, 1208–1262; c) Z. Ke, G. C. Tsui, X.-S. Peng, Y.-Y. Yeung in *Progress in Heterocyclic Chemistry*, *Vol. 28* (Eds.: G. W. Gribble, J. A. Joule), Elsevier, Amsterdam, **2016**, pp. 219–274.

[15] a) Á. Rosana, M. Claudio, M. Youssef, D. J. Gabriel, J. M. Aurrecoechea, A. R. de Lera, *Chem. Eur. J.* **2010**, *16*, 12746–12753; b) Y. Ye, R. Fan, *Chem. Commun.* **2011**, *47*, 5626–5628; c) A. Blanc, V. Beneteau, J.-M. Weibel, P. Pale, *Org. Biomol. Chem.* **2016**, *14*, 9184–9205; d) D. Sole, I. Fernandez in *Advances in Transition-Metal Mediated Heterocyclic Synthesis* (Eds.: D. Sole, I. Fernandez), Academic Press, Cambridge, MA, **2018**.

[16] a) M. Kim, S. Lee, K. Kim, D. Shin, H. Kim, H. Song, *Chem. Commun.* **2014**, *50*, 14938–14941; b) S. Seo, X. Yu, T. J. Marks, *J. Am. Chem. Soc.* **2009**, *131*, 263–276.

[17] E. Arras, A. P. Seitsonen, F. Klappenberger, J. V. Barth, *Phys. Chem. Chem. Phys.* **2012**, *14*, 15995–16001.

[18] a) J. Solomon, R. Madix, J. Stöhr, *Surf. Sci.* **1991**, *255*, 12–30; b) J. Solomon, R. Madix, J. Stöhr, *J. Chem. Phys.* **1991**, *94*, 4012–4023; c) J. A. Lloyd, A. C. Papageorgiou, S. Fischer, S. C. Oh, O. Saglam, K. Diller, D. A. Duncan, F. Allegretti, F. Klappenberger, M. Stöhr, R. J. Maurer, K. Reuter, J. Reichert, J. V. Barth, *Nano Lett.* **2016**, *16*, 1884–1889.

[19] a) A. C. Papageorgiou, S. Fischer, J. Reichert, K. Diller, F. Blobner, F. Klappenberger, F. Allegretti, A. P. Seitsonen, J. V. Barth, *ACS Nano* **2012**, *6*, 2477–2486; b) L. Smykalla, P. Shukrynau, C. Mende, H. Lang, M. Knupfer, M. Hietschold, *Chem. Phys.* **2015**, *450–451*, 39–45.

[20] J. Meisner, J. Kästner, *Angew. Chem. Int. Ed.* **2016**, *55*, 5400–5413; *Angew. Chem.* **2016**, *128*, 5488–5502.